Hindawi
Mathematical Problems in Engineering
Volume 2021, Article ID 6687064, 12 pages
https://doi.org/10.1155/2021/6687064

*Research Article*

# Investigation of Counterflow Microchannel Heat Exchanger with Hybrid Nanoparticles and PCM Suspension as a Coolant

**Mushtaq I. Hasan,[1] Mohammad J. Khafeef,[1] Omid Mohammadi ,[2] Suvanjan Bhattacharyya,[3] and Alibek Issakhov[4]**

[1]*Mechanical Engineering Department, College of Engineering, University of Thi-Qar, Nasiriyah, Iraq*
[2]*Department of Mechanical Engineering, Sharif University of Technology, Tehran, Iran*
[3]*Center for Renewable Energy and Environment Development, Department of Mechanical Engineering, Birla Institute of Technology & Science, Pilani Campus, Vidya Vihar, Pilani, Rajasthan 333 031, India*
[4]*Faculty of Mechanics and Mathematics, Department of Mathematical and Computer Modelling, Al-Farabi Kazakh National University, Almaty, Kazakhstan*

Correspondence should be addressed to Omid Mohammadi; omidmohmm@alum.sharif.edu

Received 19 November 2020; Revised 23 December 2020; Accepted 10 March 2021; Published 25 March 2021

Academic Editor: Younes Menni



The effect of the hybrid suspension on the intrinsic characteristics of microencapsulated phase change material (MEPCM) slurry used as a coolant in counterflow microchannel heat exchanger (CFMCHE) with different velocities is investigated numerically. The working fluid used in this paper is a hybrid suspension consisting of nanoparticles and MEPCM particles, in which the particles are suspended in pure water as a base fluid. Two types of hybrid suspension are used ($Al_2O_3$ + MEPCM and Cu + MEPCM), and the hydrodynamic and thermal characteristics of these suspensions flowing in a CFMCHE are numerically investigated. The results indicated that using hybrid suspension with high flow velocities improves the performance of the microchannel heat exchanger while resulting in a noticeable increase in pressure drop. Thereupon, it causes a decrease in the performance index. Moreover, it was found that the increment of the nanoparticles' concentration can rise the low thermal conductivity of the MEPCM slurry, but it also leads to a noticeable increase in pressure drop. Furthermore, it was found that as the thermal conductivity of Cu is higher than that for $Al_2O_3$, the enhancement in heat transfer is higher in case of adding Cu particles compared with $Al_2O_3$ particles. Therefore, the effectiveness of these materials depends strongly on the application at which CFMCHE is employed.

## 1. Introduction

The need for cooling devices in various industries such as building [1], electronic devices [2], and solar applications [3–6] has increased so that various researches have been conducted on this field. Thus, enhancing the performance of heat transfer and thermal storage systems is very important and has gained lots of interest [7]. The geometry and working flow are the most noteworthy methods for improvement. Using metal and carbon nanofluids, due to the high thermal conductivity of these materials, has intensified their application in modern heat transfer systems. Phase change materials (PCMs) could improve the heat storage capacity of the fluid and can enhance the heat storage and heat transfer potential of the working fluid by absorbing and releasing heat at a constant temperature. A point to be noted is that the weak thermal conductivity of PCM has limited severely the heat transfer of these materials during both discharging and charging processes in thermal storage systems. A wide range of investigations was conducted to enhance the thermal conductivity of PCMs. From these methods, the use of nanoparticles to increase the heat transfer rates is of high significance [8]. Kashani et al. [9] carried out a numerical investigation into the discharging of

Nanoenhanced Phase Change Material (NEPCM) inside an enclosure. They used different types of nanofluids at concentrations of $\phi = 0\%$, 2.5%, and 5% in a cavity in which the left wall is under constant heat flux, and the other sides were thermally insulated. It was illustrated that the heat transfer rate of the enclosure improves, as the nanoparticles are added to the system. Gujarathi [10] studied the characteristics of PCM enriched by nanoparticles to be used in a data center cooling system. Thus, wide ranges of concentration of copper were added to the paraffin as the PCM. The dispersion of nanoparticles into the paraffin increased its thermal conductivity when compared with conventional PCM. As a result, the heat transfer and melting rate were improved in the presence of nanoparticles. A point to be mentioned is that since concentration is associated with viscosity increment, the lower concentrations of nanoparticles showed better heat transfer properties in comparison with higher concentrations. Using high latent heat capacity of PCM along with high thermal conductivity of nanoparticles was stated as a promising potential in data center cooling applications. Farsani et al. [11] compared the impacts using nanoalumina at the concentration of 0.01, 0.02, and 0.03 by volume on the melting and solidification of PCM. They employed the enthalpy-porosity method to predict the PCM behavior. It was found that the overall performance of the phase change exceeds at the concentration of 0.02, which is due to the dominance of conduction improvement over the convection weakening.

In fact, dispersing carbon and metal nanoparticles into the base fluid could improve the thermal conductivity, and dispersing microencapsulated PCM (MEPCM) could enhance the heat storage capacity of the base fluid.

There are numerous studies regarding the performance of microchannel heat exchangers by using MEPCM suspension, nanofluids, and hybrid suspensions. Hasan et al. [12] numerically studied the performance of a counterflow microchannel heat exchanger (CFMCHE) charged with nanofluid as a coolant fluid. Two types of nanofluids including $Al_2O_3$-water and Cu-water were studied at concentrations of 1% to 5% by volume. It was inferred that using the nanofluids as a coolant medium results in the enhancement of the thermal performance of CFMCHE, with no rise in pressure drop because of low concentrations and also the ultrafine solid particles. The effectiveness of nanoparticles was higher in lower concentrations than in high concentrations. In other words, the effectiveness decreased with increasing the concentration. They also concluded that the best nanoparticle to be used is the one with higher thermal conductivity. Hasan [13] numerically investigated a CFMCHE with MEPCM suspension as the working fluid. The MEPCM suspension used in his research was made of microcapsules constructed from n-octadecane and polymethylmethacrylate as the core and shell materials, respectively. These capsules were dispersed in pure water at a concentration range of 0 to 20%. From their results, it was found that using MEPCM suspension as a cooling medium results in improvement of thermal performance of the CFMCHE but increasing the pressure drop significantly. As well, in order to obtain the benefits of melting of phase change material (PCM) and releasing the latent heat, it is favorable to use the MEPCM suspension with low concentration. Ho et al. [14] employed a hybrid suspension as a working fluid, consisting of $Al_2O_3$ nanoparticles and MEPCM particles and water as the base fluid. The thermal properties of hybrid suspension, including the thermal conductivity, specific heat, dynamic viscosity, latent heat of fusion, and density, were experimentally examined. It was concluded that increasing the concentration of $Al_2O_3$ nanoparticles increases the thermal conductivity of the PCM suspension. Ho et al. [15] experimentally investigated the effect of using a hybrid nanofluid on the natural convection in a circular tube. They employed pure water, PCM suspension (wPCM = 2, 5, and 10 wt.%), and nanofluids (wnp = 2, 6, and 10 wt.%) as cooling fluids and investigated the convection in the tube. The nanofluid decreased the specific heat and increased the thermal conductivity while PCM suspension weakened the thermal conductivity and increased the specific heat. The dominance of the thermal conductivity over specific heat in nanofluid and also specific heat over thermal conductivity in PCM suspension led to the improvement of the heat transfer of the working fluid. Ho et al. [16] experimentally used a hybrid nanofluid containing $Al_2O_3$ nanoparticles along with MEPCM particles to investigate their effects on the laminar convective cooling performance in a circular tube. A significant enhancement in cooling was obtained by using the hybrid nanofluid compared with the pure PCM suspension, $Al_2O_3$ nanofluid, and water. However, as the concentration rose, because of viscosity increment, the pressure drop increased, and thus, the effect of utilizing hybrid suspension decreased. Meanwhile, the dependency of pressure drop on concentration was higher in case of hybrid suspension than the nanofluid or pure PCM suspension. Elbahjaoui and El Qarnia [17] studied a shell and tube thermal storage system. They used water as the heat transfer fluid and n-octadecane embedded in shell space as the PCM. They investigated two cases of stationary and pulsating heat transfer fluid (HTF) on the storage characteristics and, thus, used nanoparticles with concentrations ranging from 0 to 7% by volume and HTF with dimensionless frequency from 0.01 to 3. The best performance was obtained in a volume fraction of 7% and pulsating frequency of 1. In the optimum case, the melting time was reduced up to 14.4%.

Augmenting convective heat transfer by using a swirl generator is one of the most popular techniques in the HVAC&R industry [18–23]. Hao and Tao [24] numerically investigated the mixed convective heat transfer. A square cavity with partial slip-filled kerosene–cobalt nanofluid is used for the study. The horizontal walls of the cavity are kept insulated while the vertical wall is partially heated. It was reported that heat flow was affected by the change in volume concentration of ferrofluid.

Goel et al. [25] numerically investigated the free convective heat transfer and flow of MHD Alumina-Cu/water nanofluid filled in a square cavity. The cavity contains a corrugated conductive cylinder. The left wall of the cavity is given constant heat. Corcione correlation is used for determining the thermal conductivity and viscosity of the hybrid nanofluid. It was reported from the results that the presence of a wavy block in the cavity influences the flow and thermal characteristics. Local Thermal Nonequilibrium model has been utilized by Tsai and Chein [26] to investigate the heat transport through convection in a porous medium filled with Ag–MgO/$H_2O$ nanofluid. The influencing parameters investigated in the study are Rayleigh number, porosity, the volume fraction of nanoparticles, interface convective heat transfer coefficient, and thermal conductivity ratio. The study concluded that vortex strength is increased with an increase in Ra while the dispersion of combined Ag–MgO nanoparticles in the fluid reduces the flow and thermal transport in the cavity as compared with Ag and MgO nanoparticles individually. Lee and Mudawar [27] numerically inspected the effect of MHD flow of second-grade fluid on the convective heat transfer in a vertical channel filled with porous medium. The results are analyzed with respect to velocity, temperature, volume concentration, skin friction, and heat and mass flow rate. It was revealed that increasing the permeability results in an increase in skin friction.

Manikandan and Rajan [28] experimentally investigated the double pipe HE, shell and tube HE, and plate HE for the same surface area under the same condition with the same nanofluids for thermal and flow characteristics. The results obtained from the experiments showed that minimum pressure drop was obtained with plate-type HE at 27% enhancement while maximum pressure was observed with double pipe HE with 85% enhancement in thermal transport. Sadeghi et al. [29] numerically revealed the benefits of using multilayer PCMs. 15 sets of experiments have been conducted to investigate the effect of various arrangements and thickness of the layer of phase change materials. It was revealed that the single layer saves 23% of inlet energy while three layers of PCM save 41% of inlet energy. Dogonchi et al. [30] utilize controlled volume-based FEM for investigating the presence of nanoparticles in a square cavity fitted with an elliptical cylinder for free convective heat transfer. The results obtained from the simulation show that, at a specific aspect ratio, enhancement in heat transfer and Nu was observed.

Ghalambaz et al. [31] numerically investigated the impact of Ag–MgO/water hybrid nanofluid filled in a square cavity fitted with a solid conductive layer at a hot wall for free convection. The parameters used for the study are volume concentration of nanoparticles, Rayleigh number, and thermal conductivity ratio. The study concluded that adding the hybrid nanoparticles in the base fluid and increasing the Ra and thermal conductivity ratio lead to the enhancement of heat transport. Ishak et al. [32] investigated the effect of wall thickness on heat transfer and entropy production in a square cavity filled with $Al_2O_3$ nanofluid. A moving heat source is present at the lower wall, which allows partial isothermal heating while other walls remain insulated. It was revealed from the obtained results that thermal conductivity and thickness of the wall are key parameters to control the optimal heat transfer and pressure drop.

Rejvani et al. [33] experimentally reveal the effect of the addition of $SiO_2$, and MWCNT in 10 W 40 engine oil. The viscosity of the resulting hybrid nanofluid was tested for various concentrations at different temperature ranges. The results show a 35% increase in the viscosity of the hybrid nanofluid comparative to base fluid.

Alsabery et al. [34] computationally studied the convective heat transfer and entropy production in a trapezoidal cavity filled with nanohomogenous $Al_2O_3$-water nanofluid under the influence of a magnetic field. The governing PDEs are solved using Galerkin weighted residual FEM. The parameters studied are Rayleigh No., the concentration of nanoparticles, Hartmann No., thermal conductivity, and height of the trapezoidal body. It was revealed that streamlines show more sensitive behavior for Hartmann as compared with the change in volume fraction.

Mehryan et al. [35] revealed the impact of MWCNT-$Fe_2O_3/H_2O$ nanofluid on the convective heat transfer under the influence of an inclined magnetic field. The parameters that influence the thermal and flow characteristics are studied. An increase in average Nusselt's number was up to $Ra = 10^4$ while an increase in viscosity due to the addition of nanoparticles decreases the average Nu. Hoseinzadeh et al. [36] numerically investigated porous rectangular fin and run the simulation for analyzing the thermal transport. The results obtained from Runge-Kutta numerical analysis are compared with results obtained through collocation method (CM), homotopy perturbation method (HPM), and homotopy analysis method (HAM). It was revealed from the study that on increasing the porosity, convection, and radiation; temperature gradient and heat flow increase along the fin length. Taamneh et al. [37] computationally investigated the thermal and flow behavior of $Al_2O_3$-$H_2O$ nanofluid in a triangular duct. The Reynolds number varied between 4000 and 10000. 20% increase in friction factor was observed with the addition of nanoparticles in comparison to base fluid while pressure drop was increased by 85% for $Re = 10000$. Besides this, a 40% increase in the production of entropy was also observed when varying the concentration of nanoparticles from 0.05 to 0.1%. Raza et al. [38] investigated the effect of $MoS_2$–$H_2O$ nanofluid in a channel with different shapes of nanoparticles. A magnetic field influenced the flow. The results obtained from the analysis show that increasing the concentration of nanoparticles in the base fluid increases the Nu while increasing the value of wall expansion ratio results in augmentation of velocity profile between bottom wall and center.

Giwa et al. [39] investigated the impact of ferrous hybrid nanofluid on the convective thermal and flow performance in the rectangular cavity under the influence of a magnetic field. The thermal properties of hybrid nanofluid are also analyzed for different particle concentrations. The magnetic field enhances the average Nu by 4.9% while increasing the strength of the magnetic field further enhances the thermal transport. The authors also noticed that the use of hybrid nanofluid shows better results in comparison to mono nanofluid. Giwa et al. [40] in another work investigated the thermal performance of Alumina-MWCNT/water nanofluid filled in a square enclosure. The nanofluid has been investigated for the different weight ratios of nanoparticles. It was revealed that nanofluid with a 60–40 weight ratio of $Al_2O_3$-MWCNT nanoparticles gives the best results. The hybrid nanofluid also promotes convective heat transfer with the cavity. Osman et al. [41] experimentally investigated a uniformly heated rectangular channel for convective heat transfer in a turbulent flow regime. Alumina-water nanofluid is used as a working fluid for the investigation. The Re varied from 200 to 7000. It was revealed from the results that a maximum heat transfer of 54% was observed in transition flow for nanofluids having 1% of nanoparticles. Mahadevi et al. [42] numerically investigated the effect of different inclination angles of the circular tube on the mixed convection heat transfer of $Al_2O_3$-water nanofluid. It was observed that maximum deposition of nanoparticles takes place at a $30^o$ inclination angle for all concentrations. It was revealed that inclination angles have a little effect on HTC up to $35^o$. Further increase in the inclination angle decreases the HTC.

Sharifpur et al. [43] optimized the concentration of $TiO_2$-water nanofluid for maximum convective heat transfer in a square cavity. The upper and lower walls of the cavity are insulated while a temperature gradient exists between the left wall and right wall. It was found that the addition of $TiO_2$ nanoparticles enhances the heat transport for all concentrations while the maximum heat transfer of 8.2% was observed at 0.05% concentration. Sharifpur et al. [44] experimentally investigate the impact of the size of $Al_2O_3$ nanoparticles on the thermal conductivity of $Al_2O_3$-glycerol nanofluid. The nanofluid prepared with 3 different sizes of nanoparticles for concentration varied between 0.5 and 4%. It was revealed from the experiments that maximum augmentation of thermal conductivity was observed at 4% concentration for 31 nm nanoparticles. It was also found that thermal conductivity is influenced by volume concentration and size of nanoparticles, while temperature variation shows negligible impact.

After a wide review of previous research, the researcher did not find a previous study regarding the usage of hybrid suspension in the heat exchanger of microchannels. Thus, it is a source of modernity for this paper. In fact, by using the hybrid suspension, both advantages of nanoparticles and microcapsules are obtained. MEPCM can improve the heat capacity of the cooling fluids, and on the other hand, nanofluid can improve the thermal conductivity; thereupon, using a mixture of these materials may lead to a significant increase in heat transfer of microchannel heat exchanger.

## 2. Mathematical Model

Figure 1 represents the schematic structure of CFMCHE used in this study with square channels carrying cold and hot fluids. To study the fully CFMCHE, numerically, a huge amount of time is required due to its complication. As shown in Figure 2, given that there is a symmetry between the cold and hot channel rows, geometrically and thermally, assuming a part of the geometry as the model studied is acceptable, since it gives an adequate indication for the whole heat exchanger performance. Hence, two channels in the cold and hot fluids flow, and the separating wall between them is considered as the studied cases and modeled numerically [18, 19].

The assumptions used to solve this model are 3D, laminar, steady-state, incompressible fluid, continuum flow, constant properties, and thermally isolated from the ambient.

## 3. Governing Equations

The governing equations are continuity, momentum, and energy used for the flow of pure fluids, nanofluid, MEPCM suspension, and hybrid suspension as follows [13, 20, 21].

*3.1. Governing Equations for Pure Water and Nanofluids*

The continuity equation is

$$\frac{\partial u_j}{\partial x}+\frac{\partial v_j}{\partial y}+\frac{\partial w_j}{\partial z}=0. \tag{1}$$

The momentum equations are

$$u_j\frac{\partial u_j}{\partial x}+v_j\frac{\partial u_j}{\partial y}+w_j\frac{\partial u_j}{\partial z}=\frac{1}{\rho_j}\frac{\partial P}{\partial x}+\frac{\mu_j}{\rho_j}\left(\frac{\partial^2 u_j}{\partial x^2}+\frac{\partial^2 u_j}{\partial y^2}+\frac{\partial^2 u_j}{\partial z^2}\right), \tag{2}$$

$$u_j\frac{\partial v_j}{\partial x}+v_j\frac{\partial v_j}{\partial y}+w_j\frac{\partial v_j}{\partial z}=\frac{1}{\rho_j}\frac{\partial P}{\partial y}+\frac{\mu_j}{\rho_j}\left(\frac{\partial^2 v_j}{\partial x^2}+\frac{\partial^2 v_j}{\partial y^2}+\frac{\partial^2 v_j}{\partial z^2}\right), \tag{3}$$

$$u_j\frac{\partial w_j}{\partial x}+v_j\frac{\partial w_j}{\partial y}+w_j\frac{\partial w_j}{\partial z}=\frac{1}{\rho_j}\frac{\partial P}{\partial z}+\frac{\mu_j}{\rho_j}\left(\frac{\partial^2 w_j}{\partial x^2}+\frac{\partial^2 w_j}{\partial y^2}+\frac{\partial^2 w_j}{\partial z^2}\right), \tag{4}$$

where $j$ stands for $h$ for the hot and $c$ for the cold fluids, respectively.

The energy equation for fluids in heat exchanger is

$$\rho c\left(u\frac{\partial T}{\partial x}+v\frac{\partial T}{\partial y}+w\frac{\partial T}{\partial z}\right)=\Phi+k\left(\frac{\partial^2 T}{\partial x^2}+\frac{\partial^2 T}{\partial y^2}+\frac{\partial^2 T}{\partial z^2}\right). \tag{5}$$

The energy equation for solid walls in heat exchanger is

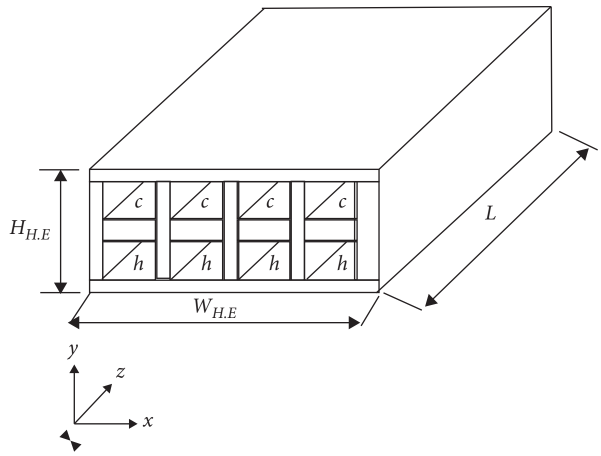


Figure 1: A schematic model of the counterflow MCHE.

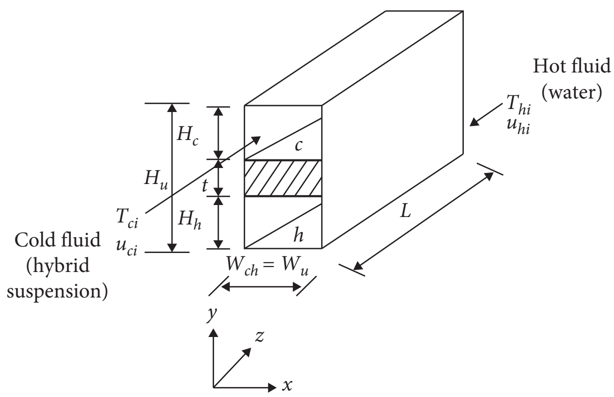


Figure 2: A schematic of the heat exchange unit.

$$k_s \nabla^2 T_s = 0. \tag{6}$$

*3.2. Governing Equations for MEPCM and Hybrid Suspensions.* The governing equations used for pure fluid (equations 1 to 4 and 6) are also used MEPCM and hybrid suspension.

The enthalpy-based energy equation is written as follows:

$$\nabla \cdot \left[ \vec{v} \left( \rho_f H_e \right) \right] = \nabla \cdot \left( k_f \nabla T_f \right). \tag{7}$$

It also can be defined as

$$\rho_f \left[ u \frac{\partial H_e}{\partial x} + v \frac{\partial H_e}{\partial y} + w \frac{\partial H_e}{\partial z} \right] = k_f \left[ \frac{\partial^2 T_f}{\partial x^2} + \frac{\partial^2 T_f}{\partial y^2} + \frac{\partial^2 T_f}{\partial z^2} \right]. \tag{8}$$

The enthalpy of the slurry ($H_e$) is shown by equation (9) and computed as follows:

$$\mathrm{He} = \mathrm{he} + \Delta H. \tag{9}$$

The sensible heat is calculated by equation (10), in which $h_{\mathrm{ref}}$ is the reference enthalpy at $T_{\mathrm{ref}}$ [21].

$$h_e = h_{\mathrm{ref}} + \int_{T_{\mathrm{ref}}}^{t} C p_f \mathrm{d}T. \tag{10}$$

The slurry's latent heat ($\Delta H$) is calculated by equation (11), where ($\beta$) is the mass ratio of molten to the total PCM in the slurry, ($\Phi$) is the MEPCM mass fraction, and ($L$) is the fusion latent heat. The PCM begins to melt at $T_{\mathrm{solidus}}$ where the liquid fraction is zero and melting ends at $\mathrm{T}_{\mathrm{liquidus}}$. At this point, the liquid fraction reaches one.

$$\Delta H = \beta \phi L, \tag{11}$$

where $\beta = 0$ if $T_f < T_{\mathrm{solidus}}$, and $\beta = 1$ if $T_f > T_{\mathrm{liquidus}}$.

$$\beta = \frac{T_f - T_{\mathrm{solidus}}}{T_{\mathrm{liquidus}} - T_{\mathrm{solidus}}}, \quad \text{if } T_{\mathrm{solidus}} < T_f < T_{\mathrm{liquidus}}. \tag{12}$$

*3.3. Model Boundary Conditions.* The working fluids enter the channels at a defined velocity and temperature. Pure water is the hot fluid used in hot channels while the cold fluid in the cold channels is tested (pure water, Nanofluid, MEPCM suspension, and hybrid suspension). The boundary conditions of the model are given in Tables 1–3.

In the present study, to solve the boundary conditions and also governing equations, the finite volume method (FVM) is employed. Computational fluid dynamics (CFD) is employed to solve the model and also determine the profile of the fluid flow, temperature, and pressure fields in the CFMCHE. Meanwhile, the dimensions of the square channel used in this model are $W = 100\,\mu$m, $H = 100\,\mu$m, $L = 10$ mm, and $t = 50\,\mu$m. $W$, $H$, $L$, and $t$ are width, channel height, length, and wall thickness, respectively.

Performance parameters have been calculated as follows.

The ratio of the experimental heat transfer to the maximum heat that is possible to be transferred is defined as heat exchanger effectiveness ($\varepsilon$).

$$\varepsilon = \frac{c_h \left( T_{hi} - T_{ho} \right)}{c_{\min} \left( T_{hi} - T_{ci} \right)} - \frac{c_c \left( T_{co} - T_{ci} \right)}{c_{\min} \left( T_{hi} - T_{ci} \right)}, \tag{13}$$

where $C_c = mCp_{\mathrm{c}}$ and $\mathrm{C}_h = mCp_{\mathrm{h.}}$

In the heat exchange cell, the total pressure drop is

$$\Delta P_t = \Delta P_h + \Delta P_c = \left( P_{hi} - P_{ho} \right) - \left( P_{ci} - P_{co} \right). \tag{14}$$

In order to investigate the overall performance of the CFMCHE, both hydrodynamic and thermal performances must be taken into account. Thus, performance index is defined as the effectiveness of CFMCHE to the total pressure drop of heat exchanger [19]:

$$\eta = \frac{\varepsilon}{\Delta pt}. \tag{15}$$

The input power required for the pump to circulate fluids in the microchannel heat exchanger is

$$PP = V \Delta Pt. \tag{16}$$

Flow rate ($\mathrm{m}^3$/s) is defined as follows:

Table 1: Bottom channel (hot fluid) ($0 \le y \le Hh$).

| Location | Boundary condition | Comments |
|---|---|---|
| At $x = 0$ | $u_h = u_{hi}$, $v_h = w_h = 0$, $T_h = T_{hi}$ | Hot fluid inflow |
| At $x = L$ | $(\partial u_h/\partial x) = v_h = w_h = 0$, $(\partial T_h/\partial x) = 0$ | Hot fluid outflow (fully developed flow, end of the channel) |
| At $y = 0$ | $u_h = v_h = w_h = 0$, $(\partial T_h/\partial y) = 0$ | No-slip, adiabatic wall |
| At $y = H_h$ | $u_h = v_h = w_h = 0$, $-k_h(\partial T_h/\partial y) = -k_s(\partial T_s/\partial y)$, $T_h = T_s$ | Fluid-solid interface (no-slip, conjugate heat transfer) |
| At $z = 0$ | $u_h = v_h = w_h = 0$, $(\partial T_h/\partial z) = 0$ | No-slip, adiabatic wall |
| At $z = W_{ch}$ | $u_h = v_h = w_h = 0$, $(\partial T_h/\partial z) = 0$ | No-slip, adiabatic wall |

Table 2: Top channel (cold fluid) ($Hh + t \le y \le Hh + t + Hc$).

| Location | Boundary condition | Comments |
|---|---|---|
| At $x = 0$ | $(\partial u_c/\partial x) = v_c = w_c = 0$, $(\partial T_c/\partial x) = 0$ | Cold fluid outflow (fully developed flow, end of the channel |
| At $x = L$ | $u_c = u_{ci}$, $v_c = w_c = 0$, $T_c = T_{ci}$ | Cold fluid inflow |
| At $y = H_h + t$ | $u_c = v_c = w_c = 0$, $-k_c(\partial T_c/\partial y) = -k_s(\partial T_s/\partial y)$, $T_c = T_s$ | Fluid-solid interface (no-slip, conjugate heat transfer) |
| At $y = H_h + t + H_c$ | $u_c = v_c = w_c = 0$, $(\partial T_c/\partial y) = 0$ | No-slip, adiabatic wall |
| At $z = 0$ | $u_c = v_c = w_c = 0$, $(\partial T_c/\partial z) = 0$ | No-slip, adiabatic wall |
| At $z = W_{ch}$ | $u_c = v_c = w_c = 0$, $(\partial T_c/\partial z) = 0$ | No-slip, adiabatic wall |

Table 3: Solid wall separating two channels ($Hh \le y \le Hh + t$).

| Location | Boundary condition | Comments |
|---|---|---|
| At $x = 0$ | $(\partial T_s/\partial x) = 0$ | Adiabatic wall |
| At $x = L$ | $(\partial T_s/\partial x) = 0$ | Adiabatic wall |
| At $y = H_h$ | $-k_h(\partial T_h/\partial y) = -k_s(\partial T_s/\partial y)$, $T_h = T_s$ | Fluid-solid interface |
| At $y = H_h + t$ | $-k_c(\partial T_c/\partial y) = -k_s(\partial T_s/\partial y)$, $T_c = T_s$ | Fluid-solid interface |
| At $z = 0$ | $(\partial T_s/\partial z) = 0$ | Adiabatic wall |
| At $z = W_{ch}$ | $(\partial T_s/\partial z) = 0$ | Adiabatic wall |

$$V = v_{in} A. \tag{17}$$

There is another factor called performance factor defined as the heat transfer rate to the pumping power ratio and used to investigate the overall performance of the CFMCHE and also verify the obtained results of the performance index [19]:

$$\eta^* = \frac{q(W)}{P \cdot P(W)}. \tag{18}$$

## 4. Properties of Fluids

*4.1. Properties of MEPCM Suspension.* MEPCM particles are made of a polymer shell surrounding a core of PCM, preventing PCM from leakage, and keeping the form during phase change. Figure 3 represents a schematic of a microcapsule during the phase change process [13]. Herein, the average diameter of MEPCM particles is 5 $\mu$m. The selection of core and shell materials of the microcapsule corresponds to the transporter fluid. N-octadecane with a melting temperature of about 301 K is used as PCM in the core of the capsule, and the shell is made up of polymethylmethacrylate (PMMA) [22–24]. Given that the physical properties of the wall material and PCM affect the properties of the MEPCM particle, different components must be taken into account while calculating the properties of MPCM.

The densities of solid and liquid PCM were assumed to be the same as the density of n-octadecane. Moreover, energy and mass balances were utilized to calculate the density and specific heat of the microcapsules, respectively [25].

$$Cp_{\mathrm{PCM}} = \frac{(7Cp_c + 3Cp_{\mathrm{wall}})p_c p_{\mathrm{wall}}}{(3p_c + 7p_{\mathrm{wall}})\rho_{\mathrm{PCM}}}, \tag{19}$$

$$\rho_{\mathrm{PCM}} = \frac{10}{7}\left(\frac{d_c}{d_{\mathrm{PCM}}}\right)^3 p_c. \tag{20}$$

The thermal conductivity of microcapsules is also represented as follows:

$$\frac{1}{k_{\mathrm{PCM}} d_{\mathrm{PCM}}} = \frac{1}{k_c d_c} + \frac{d_{\mathrm{PCM}} - d_c}{k_{\mathrm{wall}} d_{\mathrm{PCM}} d_c}. \tag{21}$$

PCM stands for the whole (capsule = wall + core) and the wall is the wall of the capsule (polymer). $C$ is the core material (PCM) and $d$ is the diameter.

The suspension properties are a function of the properties of water (base fluid) and properties of the microcapsules. Hence, the specific heat and density are determined using a mass and energy balance [22–25].

$$\rho_f = c\rho_{\mathrm{PCM}} + (1 - c)\rho_w, \tag{22}$$

$$C\rho_f = \phi c\rho_{\mathrm{PCM}} + (1 - \phi)C\rho_w. \tag{23}$$

The viscosity of the suspension is also determined using

$$\mu_f = \mu_w\left(1 - c - 1.16c^2\right)^{-2.5}. \tag{24}$$

The thermal conductivity of the suspension is calculated as

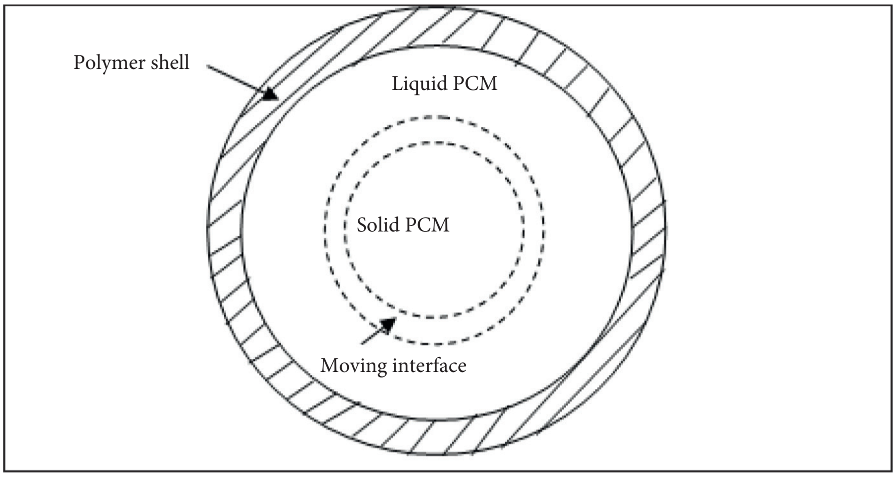


FIGURE 3: Schematic diagram of single MEPCM particles during melting.

$$k_f = \frac{2k_w + k_{PCM} + 2c(k_{PCM} - k_w)}{2 + (k_{PCM}/k_w) - c((k_{PCM}/k_w) - 1)}. \tag{25}$$

The mass fraction can be calculated from

$$\phi = \frac{c\rho_{PCM}}{(\rho_w + c(\rho_{PCM} - \rho_w))}. \tag{26}$$

*4.2. Properties of Nanofluids.* According to the previous studies [26, 27], the thermophysical properties of the nanofluids are a function of the properties of solid particles, the base fluid, particles shape, and volume fraction of the solid particles in the suspension. The properties of nanofluids are determined using the following relations:

Thermal conductivity:

$$k_{nf} = k_f\left(\frac{k_p + (SH-1)k_f(SH-1)c(k_f - k_p)}{k_p + (SH-1)k_f + c(k_f - k_p)}\right). \tag{27}$$

Viscosity:

$$\mu_{nf} = \mu_f(1 + 2.5c). \tag{28}$$

Density:

$$\rho_{nf} = c\rho_p + (1-c)\rho_f. \tag{29}$$

Specific heat:

$$C\rho_{nf} = cC\rho_p + (1-c)C\rho_f. \tag{30}$$

In equation (27), SH indicates the solid particle shape factor.

$$SH = \frac{3}{\psi}. \tag{31}$$

$\psi$ represents the ratio of the surface area of a sphere (with the same volume of the particle) to the surface area of the particle. Thus, for the spherical particles, SH is 3.

$k_p$, $k_f$, and $k_{nf}$ are thermal conductivities of the solid particles, base fluid, and nanofluid, respectively.

*4.3. Properties of Hybrid Suspensions.* To determine the viscosity and thermal conductivity properties of hybrid suspension, the following relations are used [28]:

Thermal conductivity:

$$k_{hs} = \frac{k_{nf}(1-3c)}{2}. \tag{32}$$

Viscosity:

$$\mu_{hs} = \mu_{nf}(1 + 7.85\phi). \tag{33}$$

To calculate the specific heat and density of the suspension, we use the following relations [14].

Specific heat:

$$Cp_{hs} = \left[\frac{c_{np}\rho_{np}cp_{np} + c_{MEPCM}\rho_{MEPCM}cp_{MEPCM} + (1 - c_{np} - c_{MEPCM})c\rho_{bf}p_{bf}}{p_{hs}}\right]. \tag{34}$$

Density:

$$p_{hs} = c_{np}\rho_{np} + c_{\mathrm{MEPCM}}\rho_{\mathrm{MEPCM}} + \left(1 - c_{np} - c_{\mathrm{MEPCM}}\right)p_{bf}, \quad (35)$$

where *hs*, *np*, MEPCM, and *bf* refer to hybrid suspension, nanoparticle, microencapsulated phase change material, and base fluid, respectively. In Table 4, the rheological and thermal properties of the materials employed are listed.

## 5. Numerical Model

Governing equations were transformed into algebraic equations using the finite volume method. The SIMPLE algorithm was employed to handle the mass conservation equation and get the pressure field. Computational fluid dynamic software (FLUENT 19.1) was used to determine the fields of velocity, pressure, and temperature distribution along the CFMCHE. Afterward, all the computational domain (two channels and the separating wall) was meshed with suitable size, and then using a mesh refinement process, the generated mesh was refined.

## 6. Results and Discussion

In order to investigate the effectiveness of the nanofluids, the model was firstly operated with pure water. The inlet temperatures of cold and hot fluids flowing in the channels were set as the boundary conditions with values of $T_{ci} = 293$ K and $T_{hi} = 373$ K. Then, we repeated operating the model by using nanofluid and MEPCM suspensions with volume fractions of (2%, 4%, 6%, and 8%). Noting that a core material of PCM is n-octadecane which has $T_{\mathrm{solidus}} = 297$ K and $T_{\mathrm{liquidus}} = 302$ K; also, latent heat $\Delta H = 245{,}000$ (J/kg). And then, we repeated again operating the model by adding nanoparticles of (Cu and $Al_2O_3$) with volume fractions of (2% and 4%) to the MEPCM suspension to form the hybrid suspension.

To examine the validity of the present model, the model presented by Kashani et al. [9] was solved, and a comparison was made between the obtained results and those presented by them. The numerical model that used them is a microchannel heat exchanger composed of rectangular microchannels with hydraulic diameter $D_h = 100\,\mu$m, channel height $H = 100\,\mu$m, channel width $W = 100\,\mu$m, and length $L = 10$ mm. A silicon wall with a thickness of $50\,\mu$m separates the channels, and the inlet velocity of the fluid was chosen to be $Vi = 1$ m/s.

Figure 4 illustrates the heat transfer rate distribution in terms of volume concentration for two cases of the present study and the numerical model of [9]. According to the figure, it is evident that the two models are in good agreement with each other, and the average error is 1.16% which is attributed to the end effect. Thereupon, the present model has acceptable accuracy and could be used as a reliable model to examine the impact of different nanofluids, including MEPCM and hybrid suspension on the performance of CFMCHE.

Table 4: Properties of materials.

| Material | $p$ (kg/m$^3$) | $Cp$ (J/kg.K) | $K$ (W/m.K) | M$\mu$ (kg/m.s) |
|---|---|---|---|---|
| Pure water | 981.3 | 4189 | 0.643 | 0.00059 |
| n-octadecane (MEPCM core) | solid = 850<br>liquid = 780 | 2000 | 0.18 | — |
| PMMA (MEPCM wall) | 1190 | 1470 | 0.21 | — |
| MEPCM particles | 867.2 | 1899 | 0.1643 | — |
| Cupper (cu) | 8930 | 383.1 | 386 | — |
| $Al_2O_3$ | 3600 | 765 | 36 | — |

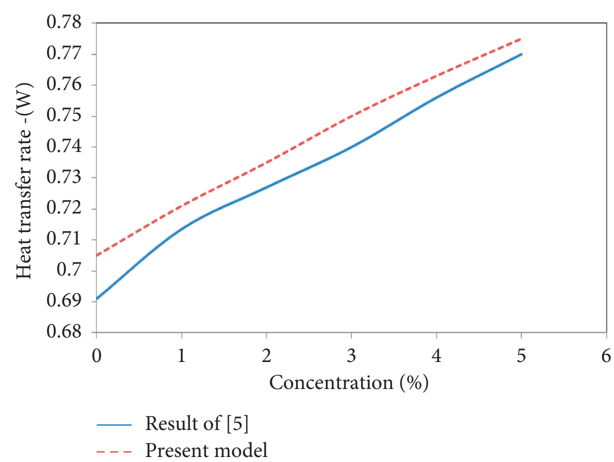


Figure 4: Variation of heat transfer rate distribution with concentration as a comparison between the present model and [5].

The heat transfer rate versus inlet velocity for pure MEPCM suspension at a concentration of 4% and enhanced (hybrid) suspension with the addition of 2% and 4% of Cu and $Al_2O_3$ nanoparticles is shown in Figure 5.

It is inferred that, for all cases, the heat transfer rate rises with increasing the velocity, which is because of the increase in flow rate. Also, results reveal that the heat transfer rises with adding nanoparticles, due to enhancing the thermal properties of suspension, especially thermal conductivity which increases with the increment of the amount of nanoparticles volume concentration. Furthermore, it could be noted that the enhancement in heat transfer is higher in case of adding Cu particles compared with $Al_2O_3$ particles because of the higher value of thermal conductivity of Cu compared with that of $Al_2O_3$.

The variation of pressure drop with inlet velocity for pure MEPCM suspension at a concentration of 4% and enhanced (hybrid) suspension with adding 2% and 4% of Cu and $Al_2O_3$ nanoparticles is portrayed in Figure 6.

From Figure 6, it is found that the pressure drop increases with the increment of inlet velocity for all cases, which is attributed to the increase in the frictional and dynamic losses. Also, it is shown that adding nanoparticles to the fluid leads to a higher pressure drop due to an increase in the dynamic

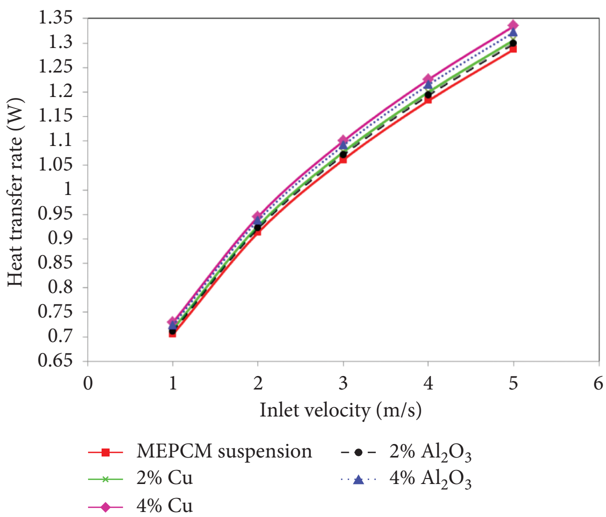


FIGURE 5: Variation of heat transfer rate with inlet velocity for different concentrations of nanoparticles at concentration 4% MEPCM suspension.

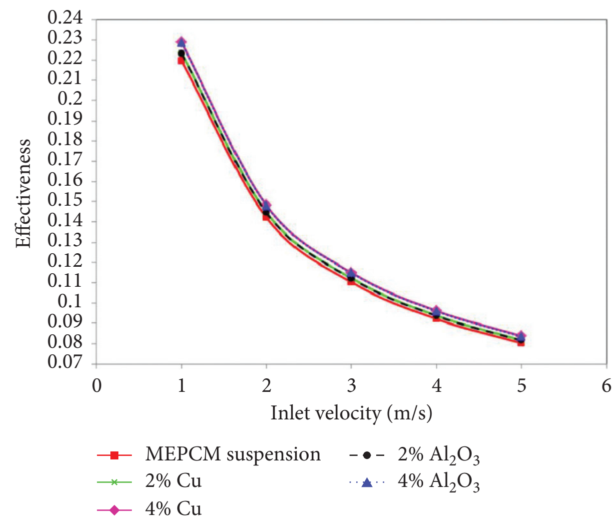


FIGURE 7: Variation of effectiveness with inlet velocity for different concentrations of nanoparticles at concentration 4% MEPCM suspension.

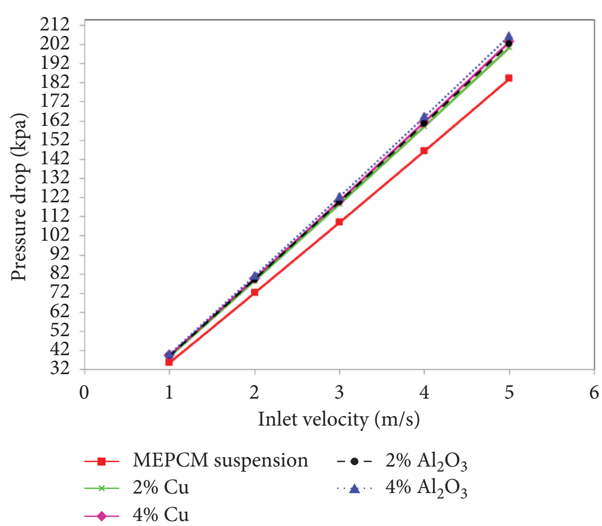


FIGURE 6: Variation of pressure drop with inlet velocity for different concentrations of nanoparticles at concentration 4% MEPCM suspension.

viscosity. This trend increased with the increment of concentration. A slight difference was discovered between pressure drop in case of adding Cu particles compared with $Al_2O_3$ particles resulting from the difference between the densities.

Figure 7 shows the effectiveness versus inlet velocity for pure MEPCM suspension (at a concentration of 4%) and enhanced (hybrid) suspension by adding 2% and 4% of Cu and $Al_2O_3$ nanoparticles, respectively.

As depicted in Figure 7, for all cases, as the inlet velocity increased, the effectiveness decreased. In fact, in high velocities, there is not enough time for all the particles to melt completely. As a result, the thermal energy was absorbed during melting, and also the effectiveness of MEPCM decreases. It is also evident that the effectiveness rises slightly with adding nanoparticles due to the enhancement of the thermal properties of suspension, especially thermal conductivity. A point to be mentioned is that, in high flow rates, the impact of nanoparticles on the development of the boundary layer decreases, resulting in better heat transfer of the suspension in higher velocities. In fact, in high velocities, the volume flow rate is dominated, and the effect of nanoparticles is weakened.

Figure 8 represents the performance index in terms of inlet velocity for pure MEPCM suspension (at a concentration of 4%) and enhanced (hybrid) suspension by adding 2% and 4% of Cu and $Al_2O_3$ nanoparticles, respectively.

As shown in Figure 8, the performance index ($\eta$) for all cases decreases with an increment of inlet velocity. It is due to the higher increment of pressure drop than effectiveness. Also, the increase in pressure drop for hybrid suspensions is higher in comparison with that of MEPCM suspension resulting in a higher performance index of MEPCM suspension than that of hybrid suspensions.

Figure 9 indicates the variation of pumping power with inlet velocity for pure MEPCM suspension at a concentration of 4% and enhanced (hybrid) suspension by adding 2% and 4% of Cu and $Al_2O_3$ nanoparticles, respectively.

From Figure 9, it is found that as the inlet velocity increases, pressure drop increases and thus pumping power rises. Also, the pumping power increases with adding nanoparticles because of the increase in dynamic viscosity that results in an increment of pressure drop. Moreover, the more the number of nanoparticles, the more pumping power. Since there is no noticeable difference between the density values of Cu and $Al_2O_3$, a slight difference was seen between pumping power in case of adding Cu particles compared with $Al_2O_3$ particles.

The variation of performance factor in terms of inlet velocity for pure MEPCM suspension (at a concentration of 4%) and enhanced (hybrid) suspension with adding 2% and 4% of Cu and $Al_2O_3$ nanoparticles is depicted in Figure 10, respectively.

It is inferred that the performance factor (□) for all cases decreases with the increment of inlet velocity since the effect

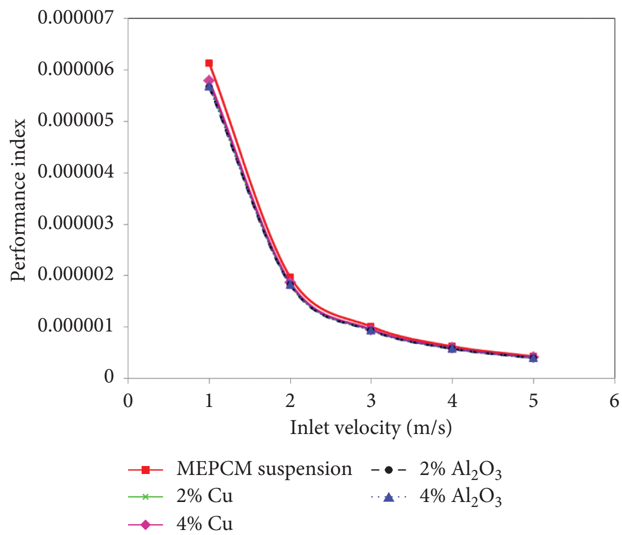


Figure 8: Variation of performance index with inlet velocity for different concentrations of nanoparticles at concentration 4% MEPCM suspension.

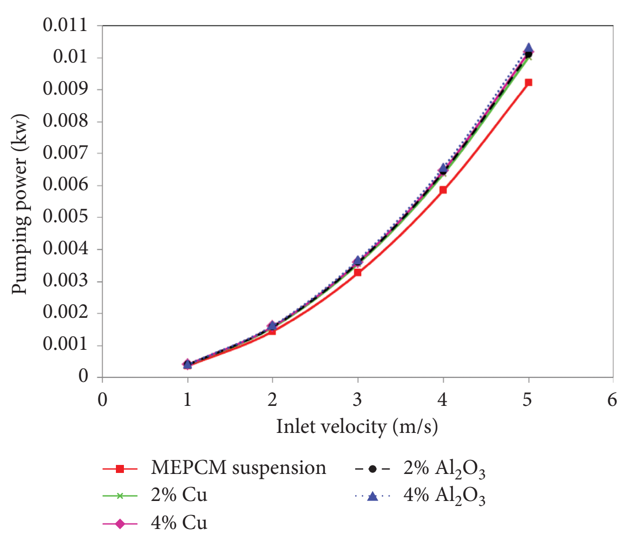


Figure 9: Variation of pumping power with inlet velocity for different concentrations of nanoparticles at concentration 4% MEPCM suspension.

of inlet velocity on the increment of pumping power is higher in comparison with that on heat transfer rate. Also, the performance factor of MEPCM suspension is higher than that of the hybrid suspensions. It is due to the higher increment of pumping power for hybrid suspensions than MEPCM suspensions.

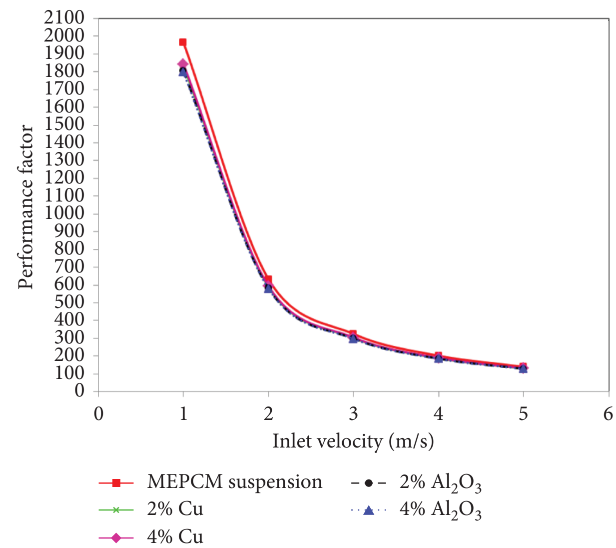


Figure 10: Variation of performance factor with inlet velocity for different concentrations of nanoparticles at concentration 4% MEPCM suspension.

## 7. Conclusions

The following conclusions are drawn:

(1) The MEPCM suspension can be enhanced by adding nanoparticles to obtain a hybrid suspension.

(2) Using higher thermal conductivity nanoparticles leads to obtaining extra enhancement in heat transfer rates for MEPCM suspension.

(3) Using hybrid suspension leads to the enhancement of heat transfer rates in CFMCHE.

(4) Also, the hybrid suspension causes an extra rise in pressure drop, which dominates the thermal performance.

(5) Using hybrid suspension with high velocities leads to an increase in heat transfer rates of the microchannel heat exchanger. On the other hand, it significantly raises the pressure drop and, hence, causes a decrease in the performance index.

## Nomenclature

$A$: Cross-sectional area ($m^2$)
C: Volume fraction%
$Cp$: Specific heat capacity (J/kg·K)
$Dh$: Hydraulic diameter (m)
$H$: Channel height (m)

He: Enthalpy of suspension (W)
he: Sensible heat (W)
$K$: Thermal conductivity (W/m K)
$L$: Heat exchanger length (m)
$M$: Mass flow rate (kg/s)
$P$: Total pressure (Pa)
$Q$: Heat transfer rate (W)
$t$: Separating wall thickness (m)
$T$: Temperature (K)
$u$: Fluid $x$-component velocity (m/s)
$v$: Fluid $y$-component velocity (m/s)
$w$: Fluid $z$-component velocity (m/s)
$x$: Axial coordinate (m)
$y$: Vertical coordinate (m)
$z$: Horizontal coordinate (m)
Wch: Channel width (m)
$\Delta P$: Pressure drop (Pa)
$\Delta H$: Latent heat (W)

*Greek letters*

$\rho$: Density (kg/m$^3$)
$\Phi$: Mass fraction
$m$: Flow rate
η: Performance index (1/Pa)
*ß*: Melted fraction
$\mu$: Dynamic viscosity (m$^2$/s)

*Subscripts*

$c$: Cold
$f$: Suspension
$h$: Hot
$i$: Inlet
ch: Channel
Max: Maximum
$o$: Outlet
$p$: Particle
$t$: Total.

## Data Availability

No data availability statement is assigned.

## Conflicts of Interest

The authors declare that they have no conflicts of interest.

## References

[1] I. Vigna, L. Bianco, F. Goia, and V. Serra, "Phase change materials in transparent building envelopes: a strengths, weakness, opportunities and threats (SWOT) analysis," *Energies*, vol. 11, no. 1, p. 111, 2018.

[2] W. Zhang, A. Maleki, A. K. Birjandi, M. Alhuyi Nazari, and O. Mohammadi, "Discrete optimization algorithm for optimal design of a solar/wind/battery hybrid energy conversion scheme," *International Journal of Low-Carbon Technologies*, vol. 60, 2020.

[3] O. A. Babar, V. K. Arora, and P. K. Nema, "Selection of phase change material for solar thermal storage application: a comparative study," *Journal of the Brazilian Society of Mechanical Sciences and Engineering*, vol. 41, no. 9, p. 355, 2019.

[4] V. Saikrishnan, A. Karthikeyan, N. Beemkumar, S. Ganesan, and D. Yuvarajan, "The thermal performance analyses of the solar energy-powered thermal energy storage system with $MgCl_2{\cdot}6H_2O$ as PCM," *Journal of the Brazilian Society of Mechanical Sciences and Engineering*, vol. 42, no. 1, p. 31, 2020.

[5] F. Moradi Gharghani, M. A. Bijarchi, O. Mohammadi, and M. B. Shafii, "An experimental investigation into a novel small-scale device for energy harvesting using vortex-induced vibration," *International Journal of Low-Carbon Technologies*, vol. 60, 2020.

[6] H. Jafari Mosleh, "A comprehensive comparative investigation on solar heating and cooling technologies from a thermo-economic viewpoint-a dynamic simulation," *Energy Science & Engineering*, vol. 9, no. 3, 2021.

[7] H. Hosseininaveh, O. Mohammadi, S. Faghiri, and M. B. Shafii, "A comprehensive study on the complete charging-discharging cycle of a phase change material using intermediate boiling fluid to control energy flow," *Journal of Energy Storage*, vol. 35, Article ID 102235, 2021.

[8] L. Selvam and D. Ramalingam, "Experimental study on the cascaded thermal energy storage system using MWCNT-enhanced phase change materials," *Journal of the Brazilian Society of Mechanical Sciences and Engineering*, vol. 41, no. 12, p. 572, 2019.

[9] S. Kashani, A. A. Ranjbar, M. Abdollahzadeh, and S. Sebti, "Solidification of nano-enhanced phase change material (NEPCM) in a wavy cavity," *Heat and Mass Transfer*, vol. 48, no. 7, pp. 1155–1166, 2012.

[10] H. Gujarathi, "Use of nanoparticle enhanced phase change material (nepcm) for data center cooling application," *Fluids*, vol. 6, no. 1, p. 31, 2017.

[11] R. Y. Farsani, A. Raisi, and A. Mahmoudi, "Successive melting and solidification of paraffin–alumina nanomaterial in a cavity as a latent heat thermal energy storage," *Journal of the Brazilian Society of Mechanical Sciences and Engineering*, vol. 41, no. 9, p. 368, 2019.

[12] M. I. Hasan, A. Rageb, and M. Yaghoubi, "Investigation of a counter flow microchannel heat exchanger performance with using nanofluid as a coolant," *Journal of Electronics Cooling and Thermal Control*, vol. 02, no. 03, pp. 35–43, 2012.

[13] M. I. Hasan, "Numerical investigation of counter flow microchannel heat exchanger with MEPCM suspension," *Applied Thermal Engineering*, vol. 31, no. 6-7, pp. 1068–1075, 2011.

[14] C. J. Ho, J. B. Huang, P. S. Tsai, and Y. M. Yang, "Preparation and properties of hybrid water-based suspension of $Al_2O_3$ nanoparticles and MEPCM particles as functional forced convection fluid," *International Communications in Heat and Mass Transfer*, vol. 37, no. 5, pp. 490–494, 2010.

[15] C. J. Ho, J. B. Huang, P. S. Tsai, and Y. M. Yang, "Water-based suspensions of $Al_2O_3$ nanoparticles and MEPCM particles on convection effectiveness in a circular tube," *International Journal of Thermal Sciences*, vol. 50, no. 5, pp. 736–748, 2011.

[16] C. Ho, J. Huang, P. Tsai, and Y. Yang, "On laminar convective cooling performance of hybrid water-based suspensions of $Al_2O_3$ nanoparticles and MEPCM particles in a circular tube," *International Journal of Heat and Mass Transfer*, vol. 54, no. 11-12, pp. 2397–2407, 2011.

[17] R. Elbahjaoui and H. El Qarnia, "Melting of nanoparticle-enhanced phase change material in a shell-and-tube latent heat storage unit heated by laminar pulsating fluid flow," *Computational Thermal Sciences: An International Journal*, vol. 9, no. 4, 2017.

[18] M. I. Hasan, M. Yaghoubi, and A. R. Abdul Muhsen, "Improving thermal performance of a counter flow microchannel heat exchanger by using nanofluid," in *Proceedings of the*

*Fourth International Conference on Thermal Engineering: Theory and Applications*, Abu Dhabi, UAE, January 2009.

[19] M. I. Hasan, A. A. Rageb, M. Yaghoubi, and H. Homayoni, "Influence of channel geometry on the performance of a counter flow microchannel heat exchanger," *International Journal of Thermal Sciences*, vol. 48, no. 8, pp. 1607–1618, 2009.

[20] M. I. Hasan and D. M. Muter, "Study the micro heat sink with pin fins and different coolants: a comparative study," *International Journal of Engineering & Technology*, vol. 7, no. 4, pp. 4856–4865, 2018.

[21] M. J. Moran, H. N. Shapiro, D. D. Boettner, and M. B. Bailey, *Fundamentals of Engineering Thermodynamics*, John Wiley & Sons, Hoboken, NJ, USA, 2010.

[22] Y. Rao, F. Dammel, P. Stephan, and G. Lin, "Convective heat transfer characteristics of microencapsulated phase change material suspensions in minichannels," *Heat and Mass Transfer*, vol. 44, no. 2, pp. 175–186, 2007.

[23] Y. Yamagishi, H. Takeuchi, A. T. Pyatenko, and N. Kayukawa, "Characteristics of microencapsulated PCM slurry as a heat-transfer fluid," *AichE Journal*, vol. 45, no. 4, pp. 696–707, 1999.

[24] Y. L. Hao and Y. X. Tao, "A numerical model for phase-change suspension flow in microchannels," *Numerical Heat Transfer, Part A: Applications*, vol. 46, no. 1, pp. 55–77, 2004.

[25] M. Goel, S. K. Roy, and S. Sengupta, "Laminar forced convection heat transfer in microcapsulated phase change material suspensions," *International Journal of Heat and Mass Transfer*, vol. 37, no. 4, pp. 593–604, 1994.

[26] T.-H. Tsai and R. Chein, "Performance analysis of nanofluid-cooled microchannel heat sinks," *International Journal of Heat and Fluid Flow*, vol. 28, no. 5, pp. 1013–1026, 2007.

[27] J. Lee and I. Mudawar, "Assessment of the effectiveness of nanofluids for single-phase and two-phase heat transfer in micro-channels," *International Journal of Heat and Mass Transfer*, vol. 50, no. 3-4, pp. 452–463, 2007.

[28] S. Manikandan and K. S. Rajan, "New hybrid nanofluid containing encapsulated paraffin wax and sand nanoparticles in propylene glycol-water mixture: potential heat transfer fluid for energy management," *Energy Conversion and Management*, vol. 137, pp. 74–85, 2017.

[29] H. M. Sadeghi, M. Babayan, and A. Chamkha, "Investigation of using multi-layer PCMs in the tubular heat exchanger with periodic heat transfer boundary condition," *International Journal of Heat and Mass Transfer*, vol. 147, p. 118970, 2020.

[30] A. S. Dogonchi, M. K. Nayak, N. Karimi, A. J. Chamkha, and D. D. Ganji, "Numerical simulation of hydrothermal features of Cu-$H_2O$ nanofluid natural convection within a porous annulus considering diverse configurations of heater," *Journal of Thermal Analysis and Calorimetry*, vol. 141, no. 5, pp. 2109–2125, 2020.

[31] M. Ghalambaz, A. Doostani, E. Izadpanahi, and A. J. Chamkha, "Conjugate natural convection flow of Ag-MgO/water hybrid nanofluid in a square cavity," *Journal of Thermal Analysis and Calorimetry*, vol. 139, no. 3, pp. 2321–2336, 2020.

[32] M. S. Ishak, A. I. Alsabery, A. Chamkha, and I. Hashim, "Effect of finite wall thickness on entropy generation and natural convection in a nanofluid-filled partially heated square cavity," *International Journal of Numerical Methods for Heat and Fluid Flow*, vol. 30, no. 3, pp. 1518–1546, 2020.

[33] M. Rejvani, S. Saedodin, S. M. Vahedi, S. Wongwises, and A. J. Chamkha, "Experimental investigation of hybrid nano-lubricant for rheological and thermal engineering applications," *Journal of Thermal Analysis and Calorimetry*, vol. 138, no. 2, pp. 1823–1839, 2019.

[34] A. I. Alsabery, R. Mohebbi, A. J. Chamkha, and I. Hashim, "Impacts of magnetic field and non-homogeneous nanofluid model on convective heat transfer and entropy generation in a cavity with heated trapezoidal body," *Journal of Thermal Analysis and Calorimetry*, vol. 138, no. 2, pp. 1371–1394, 2019.

[35] S. A. M. Mehryan, M. Izadi, Z. Namazian, and A. J. Chamkha, "Natural convection of multi-walled carbon nanotube-$Fe_3O_4$/water magnetic hybrid nanofluid flowing in porous medium considering the impacts of magnetic field-dependent viscosity," *Journal of Thermal Analysis and Calorimetry*, vol. 138, no. 2, pp. 1541–1555, 2019.

[36] S. Hoseinzadeh, P. S. Heyns, A. J. Chamkha, and A. Shirkhani, "Thermal analysis of porous fins enclosure with the comparison of analytical and numerical methods," *Journal of Thermal Analysis and Calorimetry*, vol. 138, no. 1, pp. 727–735, 2019.

[37] Y. Taamneh, A. E. Kabeel, N. Prakash, R. Sathyamurthy, and A. J. Chamkha, "Thermal and hydraulic characteristics of a triangular duct using an $Al_2O_3$ nanofluid in a turbulent flow regime," *Heat Transfer-Asian Research*, vol. 48, no. 6, pp. 2639–2654, 2019.

[38] J. Raza, F. Mebarek-Oudina, and A. J. Chamkha, "Magnetohydrodynamic flow of molybdenum disulfide nanofluid in a channel with shape effects," *Multidiscipline Modeling in Materials and Structures*, vol. 15, no. 4, pp. 737–757, 2019.

[39] S. O. Giwa, M. Sharifpur, and J. P. Meyer, "Effects of uniform magnetic induction on heat transfer performance of aqueous hybrid ferrofluid in a rectangular cavity," *Applied Thermal Engineering*, vol. 170, p. 115004, 2020.

[40] S. O. Giwa, M. Sharifpur, and J. P. Meyer, "Experimental study of thermo-convection performance of hybrid nanofluids of $Al_2O_3$-MWCNT/water in a differentially heated square cavity," *International Journal of Heat and Mass Transfer*, vol. 148, p. 119072, 2020.

[41] S. Osman, M. Sharifpur, and J. P. Meyer, "Experimental investigation of convection heat transfer in the transition flow regime of aluminium oxide-water nanofluids in a rectangular channel," *International Journal of Heat and Mass Transfer*, vol. 133, pp. 895–902, 2019.

[42] M. Mahdavi, I. Garbadeen, M. Sharifpur, M. H. Ahmadi, and J. P. Meyer, "Study of particle migration and deposition in mixed convective pipe flow of nanofluids at different inclination angles," *Journal of Thermal Analysis and Calorimetry*, vol. 135, no. 2, pp. 1563–1575, 2019.

[43] M. Sharifpur, A. B. Solomon, T. L. Ottermann, and J. P. Meyer, "Optimum concentration of nanofluids for heat transfer enhancement under cavity flow natural convection with $TiO_2$-water," *International Communications in Heat and Mass Transfer*, vol. 98, pp. 297–303, 2018.

[44] M. Sharifpur, N. Tshimanga, J. P. Meyer, and O. Manca, "Experimental investigation and model development for thermal conductivity of $\alpha$-$Al_2O_3$-glycerol nanofluids," *International Communications in Heat and Mass Transfer*, vol. 85, pp. 12–22, 2017.